Cell, Vol. 107, 513–523, November 16, 2001, Copyright ©2001 by Cell Press

LDL Receptor-Related Protein 5 (LRP5) Affects Bone Accrual and Eye Development

Yaoqin Gong,[2] Roger B. Slee,[2] Naomi Fukai, Georges Rawadi, Sergio Roman-Roman, Anthony M. Reginato, Hongwei Wang, Tim Cundy, Francis H. Glorieux, Dorit Lev, Margaret Zacharin, Konrad Oexle, Jose Marcelino, Wafaa Suwairi, Shauna Heeger, George Sabatakos, Suneel Apte, William N. Adkins, Jeremy Allgrove, Mine Arslan-Kirchner, Jennifer A. Batch, Peter Beighton, Graeme C. M. Black, Richard G. Boles, Laurence M. Boon, Carla Borrone, Han G. Brunner, Georges F. Carle, Bruno Dallapiccola, Anne De Paepe, Barbara Floege, Melissa Lees Halfhide, Bryan Hall, Raoul C. Hennekam, Tatsuo Hirose, Ab Jans, Harald Jüppner, Chong Ae Kim, Kim Keppler-Noreuil, Alfried Kohlschuetter, Didier LaCombe, Marie Lambert, Emmanuelle Lemyre, Tom Letteboer, Leena Peltonen, Rajkumar S. Ramesar, Marta Romanengo, Hannu Somer, Elisabeth Steichen-Gersdorf, Beat Steinmann, Beth Sullivan, Andrea Superti-Furga, Walter Swoboda, Marie-José van den Boogaard, Wim Van Hul, Miikka Vikkula, Marcela Votruba, Bernhard Zabel, Teresa Garcia, Roland Baron, Bjorn R. Olsen, and Matthew L. Warman[1]
The Osteoporosis-Pseudoglioma Syndrome Collaborative Group[3]

Summary

In humans, low peak bone mass is a significant risk factor for osteoporosis. We report that *LRP5*, encoding the low-density lipoprotein receptor-related protein 5, affects bone mass accrual during growth. Mutations in *LRP5* cause the autosomal recessive disorder osteoporosis-pseudoglioma syndrome (OPPG). We find that OPPG carriers have reduced bone mass when compared to age- and gender-matched controls. We demonstrate *LRP5* expression by osteoblasts in situ and show that LRP5 can transduce Wnt signaling in vitro via the canonical pathway. We further show that a mutant-secreted form of LRP5 can reduce bone thickness in mouse calvarial explant cultures. These data indicate that Wnt-mediated signaling via LRP5 affects bone accrual during growth and is important for the establishment of peak bone mass.

Introduction

In humans, bone mass increases during growth and peaks by the third decade of life (Lu et al., 1996). Later in life when bone catabolism supersedes anabolism, the significant loss of bone mass (osteoporosis) becomes a common medical problem (Riggs and Melton, 1986). In the United States, it is estimated that $10–$15 billion are spent annually for the treatment of osteoporotic fractures (NIH Consensus Development Panel on Osteoporosis Prevention, 2001). The worldwide annual incidence of osteoporotic hip fracture exceeds 1.7 million cases (http://www.who.int/inf-pr-1999/en/pr99-58.html). Numerous factors have been implicated in the development of osteoporosis. Family and epidemiological studies indicate that the peak bone mass attained during growth is an important risk factor (NIH Consensus Development Panel on Osteoporosis Prevention, 2001; Seeman et al., 1994).

Two principal cell types are responsible for the deposition and degradation of bone matrix. The bone-forming cells, osteoblasts, differentiate from mesenchymal stem cells at sites of membranous bone formation, in periosteum of endochondral bones, and in bone marrow stroma (Aubin, 1998). The bone-degrading cells, osteoclasts, differentiate from hematopoietic mononuclear cells present in peripheral blood and bone marrow (Roodman, 1996). In order for bone mass to accrue during the growth and maturation of the skeleton, bone formation by osteoblasts must exceed bone degradation by osteoclasts.

Children with the autosomal recessive disorder osteoporosis-pseudoglioma syndrome (OPPG) (Gong et al., 1996) have very low bone mass and are prone to developing fractures and deformation (Figures 1A and 1B). In contrast to other heritable childhood disorders that affect bone strength, patients with OPPG do not have identifiable defects in collagen synthesis, anabolic and catabolic hormones, calcium homeostasis, endochondral growth, or bone turnover (Gong et al., 1996). Histological analyses of bone biopsies from affected patients reveal deficient trabecular bone volume (Figures 1D and 1E) but normal surface density and appearance of osteoblasts and osteoclasts on bone surfaces (data not shown). Intriguingly, obligate carriers of OPPG mutations (i.e., parents of affected children) have been suggested to have an increased incidence of osteoporosis-related fractures. In addition to the skeletal phenotype, individuals with OPPG have eye involvement (Figure 1C). Many patients with OPPG are born with severe disruption of ocular structure, phthisis bulbi. However, persistent hyperplasia of the primary vitreous (PHPV) has been observed in children with milder eye involvement, leading to speculation that ocular pathology results from failed regression of the primary vitreal vasculature during fetal growth.

Using the positional candidate approach, we have identified the gene responsible for OPPG as being the LDL receptor-related family member *LRP5*. We show that obligate carriers of mutant *LRP5* genes have reduced bone mass when compared to age- and gender-matched controls. We demonstrate that *LRP5* is expressed by osteoblasts in situ and that its expression pattern changes over time when pluripotent mesenchy-

[1] Correspondence: mlw14@po.cwru.edu
[2] These authors contributed equally to this work.
[3] Authors' affiliations are provided at http://www.cell.com/cgi/content/full/107/4/513/DC1.

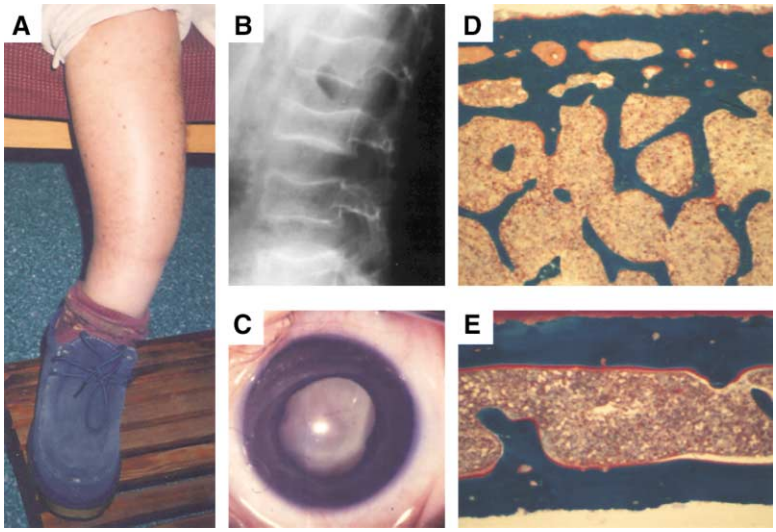

Figure 1. Clinical Features of the Osteoporosis-Pseudoglioma Syndrome

(A) Lower extremity photograph of a 40-year-old female OPPG patient demonstrating angular deformity of the tibia and fibula, the consequence of multiple fractures occurring during childhood.

(B) Lateral lumbar spine radiograph of a 10-year-old male OPPG patient demonstrating abnormal flattening and concavity of the lumbar vertebrae. Affected individuals have normal growth during the first few years of life, but can fall below the normal range for height because of long bone fractures and vertebral collapse.

(C) Photograph of the right eye of a 3-month-old male with OPPG demonstrating leukocoria (a white mass behind the pupil resembling retinoblastoma but actually a retrolental membrane). This individual had persistence of the tunica vasculosa partially covering the anterior lens surface, and evaluation of the dense retrolental membrane revealed a vascular central stalk that extended from the optic nerve into the vitreous cavity.

(D and E) Iliac crest bone biopsies (both at 40× magnification) from an unaffected 2.5-year-old child (control) and from a 2.5-year-old child with OPPG, respectively. The control biopsy is substantially thicker than the OPPG biopsy. Note that the bone volume in the control (D) allows for only one cortical surface and a substantial trabecular bone network to be contained within the microscopic field. In contrast, both the inner and outer cortices and very little trabecular bone are contained within the field of the OPPG patient (E).

mal cells are differentiated along the osteoblastic lineage in vitro. We show that LRP5 is able to mediate Wnt signaling in vitro via the canonical pathway and that dominant-negative forms of LRP5 can interfere with this process. Lastly, we show that dominant-negative forms of LRP5 can affect bone thickness in mouse calvarial explant cultures. These data indicate that LRP5 affects the accrual of bone mass during Wnt-mediated osteoblastic proliferation and differentiation.

Results

Mutations in *LRP5* Cause OPPG

Twenty-eight families affected by OPPG participated in this study. The genetic mapping of OPPG has been described (Gong et al., 1996). We found that genomic sequence from three overlapping 11q13 large insert clones (GenBank accession numbers AC024126, AC024123, and AC024124) contained three simple sequence-repeat polymorphisms (D11S1337, D11S4087, and D11S4178) as well as exons coding for LRP5. Because one nonconsanguineous OPPG family had a single affected child who was homozygous for all three SSRP markers, we hypothesized that this individual is homozygous for an ancestral haplotype that also contains an OPPG disease-causing mutation. Therefore, we sequenced the *LRP5* gene.

LRP5 cDNA contains a 4.9 kb open reading frame (Chen et al., 1999; Dong et al., 1998; Hey et al., 1998; Kim et al., 1998). Comparison of the *LRP5* cDNA with the genome sequences deposited in GenBank (see above) indicates that *LRP5* comprises 23 coding exons that span >100 kb. Surprisingly, we also identified an unprocessed pseudogene containing exons 3–9 on human chromosome 22 (GenBank accession number AL022324). Patient-derived fibroblast or EBV-transformed lymphoblastic cell lines were available from four unrelated families. We employed RT-PCR to amplify and sequence the coding region of the *LRP5* cDNA in the patients from these families, and we identified putative disease-causing mutations in each sample (Figure 2A). We confirmed that the mutations were homozygous and inherited by using the patients' and their parents' genomic DNA. We then began performing an exon-by-exon search for disease-causing mutations in the remaining families. To date, we have identified a total of six different homozygous frameshift or nonsense mutations in affected offspring from consanguineous families (Figure 2A). We have also found homozygous missense mutations in affected patients from two other consanguineous families and heterozygous nonsense, frameshift, and missense mutations in affected patients from four nonconsanguineous families (Figure 2A). The nonconsanguineous patients likely have a second mutant allele that we have not yet detected since their parents (who are also heterozygous for the mutations) do not have OPPG. Neither these mutations nor a shared haplotype were observed among the remaining families, suggesting that there is not a common ancestral mutation or a mutational hotspot. Putative disease-causing missense mutations have not been found in control DNA samples; however, we have not yet determined that they are disease causing by means of a functional assay.

Two affected siblings are homozygous for a nonsense codon within the signal peptide domain of LRP5. This would suggest that loss-of-LRP5 function is the mechanism of mutational effect in OPPG. Because other nonsense and frameshift mutations occurred within the receptor's extracellular domain, it remains possible that OPPG could also result from a dominant-negative mechanism by allowing a ligand binding portion of the receptor to be secreted and act as a decoy. To test this latter hypothesis, we transiently transfected COS-7 cells with

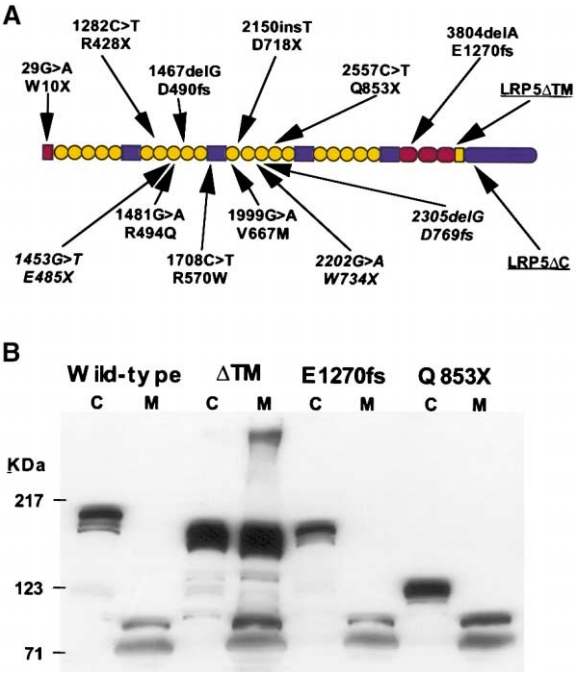

Figure 2. OPPG Is Caused by Mutation in *LRP5*

(A) The predicted structure of wild-type LRP5 is depicted. LRP5 contains a 29 amino acid signal peptide (red rectangle), 20 YWTD spacer repeat domains (yellow circles) interspersed by four EGF-like domains (blue rectangles), three LDL receptor-like ligand binding domains (red ovals), a transmembrane domain (yellow rectangle), and a 200 amino acid residue cytoplasmic domain (blue oval). Six disease-causing, homozygous frameshift and nonsense mutations and their predicted effects upon the polypeptide sequence are shown above the diagram. Putative disease-causing homozygous missense mutations are shown below the diagram, as are heterozygous mutations (in italics) found in affected individuals from nonconsanguineous unions. Mutation nomenclature follows recent recommendations (http://www.dmd.nl/mutnomen.html). The locations of the two dominant-negative LRP5 constructs (LRP5ΔTM and LRP5ΔC) are underlined.

(B) Cell lysates (C) and conditioned media (M) from transiently transfected COS-7 cells were separated on a 4%–20% gradient SDS-PAGE gel under reducing conditions and immunodetected with anti-FLAG antibody. Transfection constructs included wild-type LRP5 (Wild-type), a secreted form of LRP5 that lacks the transmembrane and cytoplasmic domains (ΔTM), and two OPPG mutants E1270fs and Q853X. Wild-type contains the transmembrane domain and is found in the cell lysate. ΔTM, which lacks the transmembrane domain, is secreted and recoverable from the conditioned media. Neither E1270fs nor Q853X, which also lack the transmembrane domain, are recoverable from conditioned media, indicating that they are synthesized but not secreted. These mutant proteins might not even be synthesized in vivo due to nonsense-mediated mRNA decay.

mammalian expression constructs containing either wild-type LRP5 (wt) or the disease-causing alleles E1270fs and Q853X to see if the mutant polypeptides were capable of being secreted. As shown in Figure 2B, these mutant proteins are synthesized but not secreted by COS-7 cells, indicating that they are unlikely to act via a dominant-negative mechanism. Given the similarity in phenotype among patients with OPPG, we speculate that OPPG disease-causing alleles are loss-of-function. However, we were able to create an artificial LRP5 construct that lacks the transmembrane domain (LRP5ΔTM) and could be secreted (Figures 2A and 2B). This indicates that mutations in LRP5 may also be able to cause disease via a dominant-negative mechanism; however, the phenotype caused by this type of mutation could be distinct from that observed in OPPG.

OPPG Carriers Also Have Reduced Bone Mass

We measured lumbar spine areal bone mineral density (aBMD) in 17 patients, 6 unaffected siblings, and 20 parents (Table 1). We considered all parents of OPPG patients as well as all unaffected siblings who had one copy of an OPPG mutant allele or haplotype to be obligate carriers. When compared to age- and gender-matched controls, all OPPG patients had extremely low aBMD ($p < 0.0001$). The average aBMD for the 23 obligate carriers was also significantly below the control mean ($p < 0.001$). These results indicate that OPPG disease-causing mutations in *LRP5* can have dominant effects as well as recessive effects.

Lrp5 Is Expressed by Osteoblasts

We performed in situ hybridization on skeletal elements in developing mice to determine possible sites of action of Lrp5 during bone formation. The lateral half of the mouse clavicle ossifies by membranous ossification beginning on embryonic day 14.0, while the medial half ossifies later by endochondral ossification (Huang et al., 1997). As shown in Figure 3A, we first detect skeletal expression of *Lrp5* in the cells that are forming the lateral part of the clavicle. These cells express other markers of skeletal differentiation, such as alkaline phosphatase and *Runx2* (data not shown), although they have not yet begun to make a detectable mineralized matrix. During embryonic day 16.5 when the diaphyseal bone collar is forming around the humerus, *Lrp5* expression is noted in osteoblasts along the endosteal surface and not in growth plate chondrocytes (Figure 3B). In addition to the detection of osteoblastic expression in appendicular bones, expression was also noted in osteoblasts that line the developing calvaria (Figure 3C). Postnatally, *Lrp5* expression was observed in trabecular and cortical osteoblasts in the appendicular skeleton in a 4-week-old mouse (data not shown).

LRP5 Expression Increases during BMP2-Induced Differentiation of the ST2 Pluripotent Mesenchymal Cell Line along the Osteoblastic Lineage

Pluripotent marrow stromal cell lines are capable of being induced along an osteoblastic lineage by the addition of exogenous growth factors (Katagiri et al., 1994; Yamaguchi et al., 1996). The addition of 300 ng/ml of BMP2 to confluent ST2 cells results in the expression of several genes that are associated with osteoblastic differentiation (Figure 4) (Aubin, 1998). *Lrp5* and *Lrp6* have low levels of expression in untreated ST2 cells. However, BMP2 addition causes a significant increase in *Lrp5* and *Lrp6* expression by 48 hr. This increased expression persists after other markers of osteoblastic differentiation (*Alpl*, *Col1a1*, and *Bglap*) have diminished. It is interesting that the increased *Lrp5* expression occurs in cells that are beginning to express the more differentiated osteoblastic phenotype. Since cells are

Table 1. Quantitative Lumbar Spine Areal Bone Mineral Density in OPPG Patients and First-Degree Relatives

Subjects		Number	Families	Sex (M/F)	Age Range (Years)	Bone Mineral Density Z Score	
						Mean (SD)	Median (Range)
OPPG	patients	17	12	9/8	2–46	−4.7 (0.9)	−5.0 (−3.1 to −6.1)
Obligate carriers	parents	20	11	10/10	36–73	−1.3 (1.4)	−1.7 (+2.7 to −3.3)
	siblings	3	3	1/2	13–20	−2.3 (0.3)	−2.1 (−2.1 to −2.6)
	all	23	11	11/12	13–73	−1.4 (1.4)	−1.7 (+2.7 to −3.3)
Noncarriers	siblings	3	2	3/0	12–26	1.0 (1.2)	1.4 (+1.9 to −0.3)

still proliferating when *Lrp5* expression begins to increase at 24 hr, we cannot rule out the possibility that Lrp5 has a role in regulating the proliferation of these pre- and early osteoblasts. However, the observation that increased *Lrp5* expression persists throughout the later stages of osteoblastic differentiation suggests a role for the receptor during terminal differentiation. We do not yet know the significance of the observation that *Lrp6* expression in this in vitro system appears to mirror that of *Lrp5*.

LRP5 Is Involved in Wnt-Mediated Signaling in Pluripotent Mesenchymal Cells that Can Be Induced along the Osteoblastic Lineage

Studies in mouse, *Drosophila*, and *Xenopus* suggest that LRP6 serves as a coreceptor with Frizzled family members during Wnt-mediated signaling (Pinson et al., 2000; Tamai et al., 2000; Wehrli et al., 2000). In the *Xenopus* axis duplication assay, LRP5 is also capable of mediating Wnt signaling (Tamai et al., 2000). Furthermore, in mammalian cells, LRP5 is capable of functioning as a Wnt coreceptor in the canonical signaling pathway that employs β-catenin as a downstream effector (Mao et al., 2001). It has also been shown that the Wnt antagonist Dickkopf interferes with Wnt signaling by binding to LRP5 and LRP6 (Bafico et al., 2001; Semenov et al., 2001). Because of the strong skeletal phenotype associated with *LRP5* mutations, we examined the effects of Wnt and LRP5 in cells that can differentiate along the osteoblastic lineage in vitro. We performed transient transfection experiments using different Wnts and studied the induction in expression of the osteoblastic markers alkaline phosphatase (ALP), *Bglap*, and *Runx2* in the pluripotent mesenchymal cells C3H10T1/2 and ST2. Wnt3a was able to induce ALP activity in both cell lines (Figures 5A and 5B) without having a significant effect on *Bglap* or *Runx2* gene expression (data not shown). This effect was inhibited by coexpression with a dominant-negative form of *Disheveled*, a downstream participant in the canonical Wnt signaling pathway (data not shown). Wnt1 and Wnt2, which also signal via the canonical pathway, also increased ALP activity (data not shown). However, Wnt5a and Wnt4, which neither elevate the level of cytosolic β-catenin nor activate LEF1-dependent transcriptional activity (Shimizu et al., 1997), did not increase ALP activity in C3H10T1/2 and ST2 cells (Figures 5A and 5B; Wnt4 data not shown). Further support for the role of the canonical Wnt signaling pathway in this process is the ability of a constitutive active mutant form of β-catenin (β-catenin*)

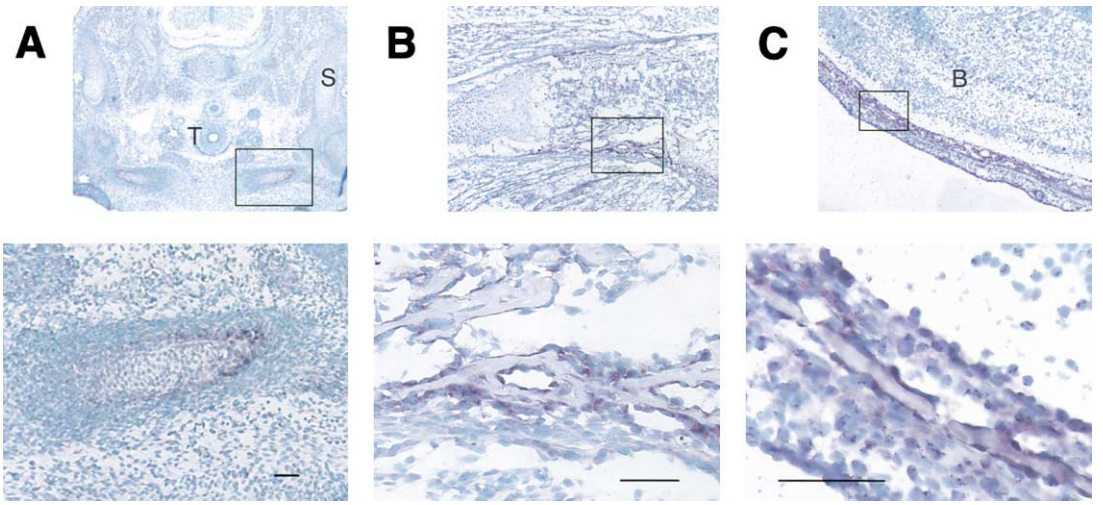

Figure 3. In Situ Hybridization Reveals *Lrp5* Expression in Skeletal Elements of the Developing Mouse Embryo

The boxes in the upper panels correspond to the magnified areas in the lower panels. The size bars indicate 50 μm.

(A) *Lrp5* expression is noted in differentiating osteoblasts that contribute to the lateral membranous part of clavicle at embryonic day 13.5 (T, trachea; S, scapula). Note that the medial portion of the clavicle, which will ossify later by endochondral ossification, does not express detectable levels of *Lrp5*, nor does the later-ossifying scapula.

(B) Osteoblasts lining the bony trabeculae of the humerus at embryonic day 16.5 and not in growth plate chondrocytes.

(C) Osteoblasts on both surfaces of the temporal bone at embryonic day 17.5 (B, brain).

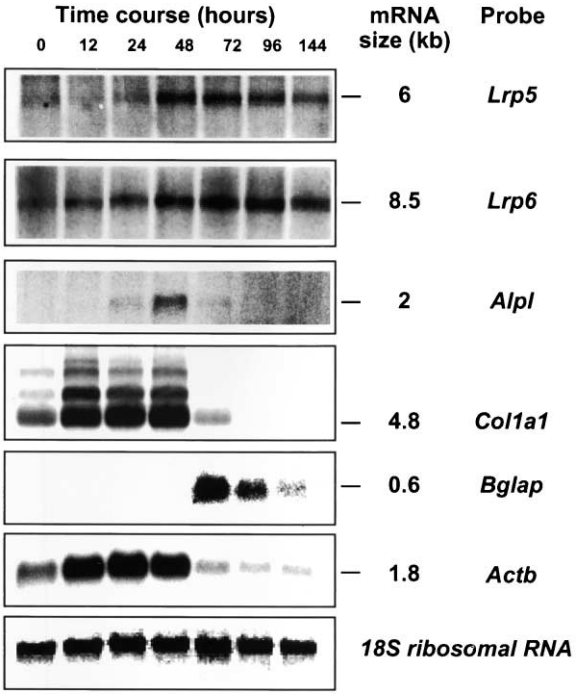

Figure 4. BMP2 Induces Changes in the Expression of *Lrp5*, *Lrp6*, and Other Markers of Osteoblastic Differentiation in Cultured ST2 Cells

Total RNA (5 μg) from untreated ST2 cells (0 hr time point) or from cells exposed to 300 ng/ml BMP2 for 12, 24, 48, 72, 96, and 144 hr were Northern blotted. cDNA probes included *Lrp5*, its closest mammalian paralog *Lrp6*, alkaline phosphatase (*Alpl*), the α1 chain of the type I collagen (*Col1a1*), osteocalcin (*Bglap*), and β actin (*Actb*). An ethidium bromide-stained 18S ribosomal RNA band demonstrates equivalent loading across lanes. Low levels of *Lrp5* and *Lrp6* expression are detected in untreated ST2 cells; expression levels increase over time, but are still low when compared to other mRNA species depicted in this figure. For example, the *Lrp5* and *Lrp6* panels represent exposure to a phosphorimager screen for 4 days, whereas the *Col1a1* panel represents only a 0.5 hr exposure.

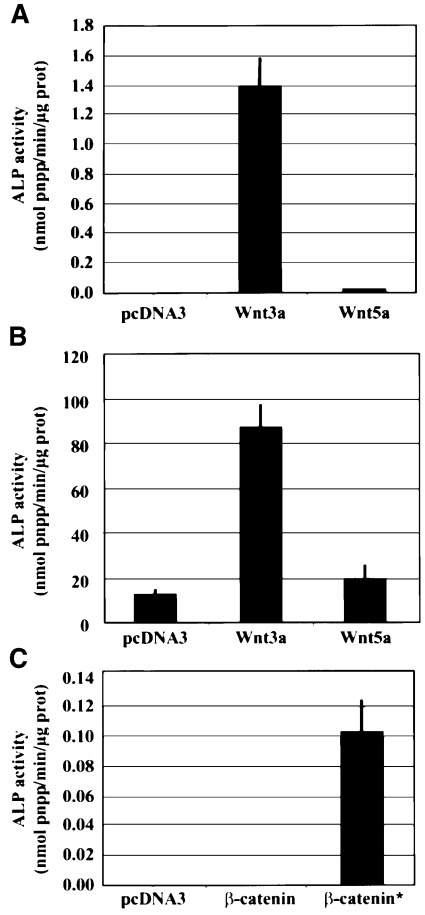

Figure 5. Wnt/β-Catenin Induces Alkaline Phosphatase (ALP) Activity in C3H10T1/2 and ST2 Cells

(A) C3H10T1/2 and (B) ST2 cells were transiently transfected with empty vector (pcDNA3.1), Wnt3a, or Wnt5a expression constructs. ALP activity was measured in cell lysates 72 hr after transfection, normalized to protein content, and expressed as nmol pnpp/min/μg of protein. Wnt 3a, but not Wnt 5a, increases ALP activity in both cell lines.

(C) C3H10T1/2 cells were transiently transfected with empty vector, wild-type β-catenin (β-catenin), or a constitutive active form of β-catenin (β-catenin*) expression constructs. ALP activity was measured in cell lysates 72 hr after transfection, normalized to protein content, and expressed as nmol pnpp/min/μg of protein. The stable mutant form of β-catenin is able to increase ALP activity. All experiments were performed in triplicate and repeated three times. Data ± one SD from one representative experiment is presented.

(Morin et al., 1997) to also induce ALP activity in C3H10T1/2 and ST2 cells (Figure 5C).

Since LRP5 is expressed in pluripotent cells that can be induced along the osteoblastic lineage, we assessed the effect of overexpression of LRP5 on Wnt3a-mediated induction of ALP activity. By using COS-7 cells, we first showed that LRP5 overexpression enhances Wnt3a-mediated TCF-1 activation (Figure 6A); however, by using C3H10T1/2 or ST2 cells, we could not show an effect of LRP5 overexpression on Wnt3a induction of ALP (Figure 6B). This may be because the concentration of downstream effectors of LRP5-mediated signaling in these cells is limiting. Therefore, we explored the consequence of a loss-of-LRP5 function in these cells. It has been reported that a secreted form of LRP5 can bind Wnt and that an LRP5 mutant lacking the cytoplasmic tail can function as a dominant negative (Mao et al., 2001). We therefore made two different constructs in which the cytoplasmic tail (LRP5ΔC) or the transmembrane domain and cytoplasmic tail (LRP5ΔTM) were deleted. LRP5ΔC and LRP5ΔTM did not enhance Wnt3a-induced TCF-1 activation in cotransfection experiments conducted in COS-7 cells (Figure 6A). Importantly, these two dominant-negative forms decreased ALP activity induced by Wnt3a in both C3H10T1/2 and ST2 cells (Figure 6B), strongly suggesting that LRP5 modulates the inducing effect of Wnt3a. We then tested if dominant-negative LRP5 constructs could affect the induction of ALP by stimuli other than Wnt. Interestingly, LRP5ΔC and LRP5ΔTM significantly inhibited the induction of ALP by BMP2 in ST2 (Figure 6C) and C3H101/2 cells (data not shown). Moreover, ST2 cells that were stably expressing LRP5ΔC (LRP5ΔC-ST2) were less able to express ALP in response to either Wnt3a (Figure 6D) or BMP2 (data not shown), compared to ST2 cells stably expressing wild-type LRP5 (LRP5-ST2). However, when we overexpressed the constitutive active β-catenin mu-

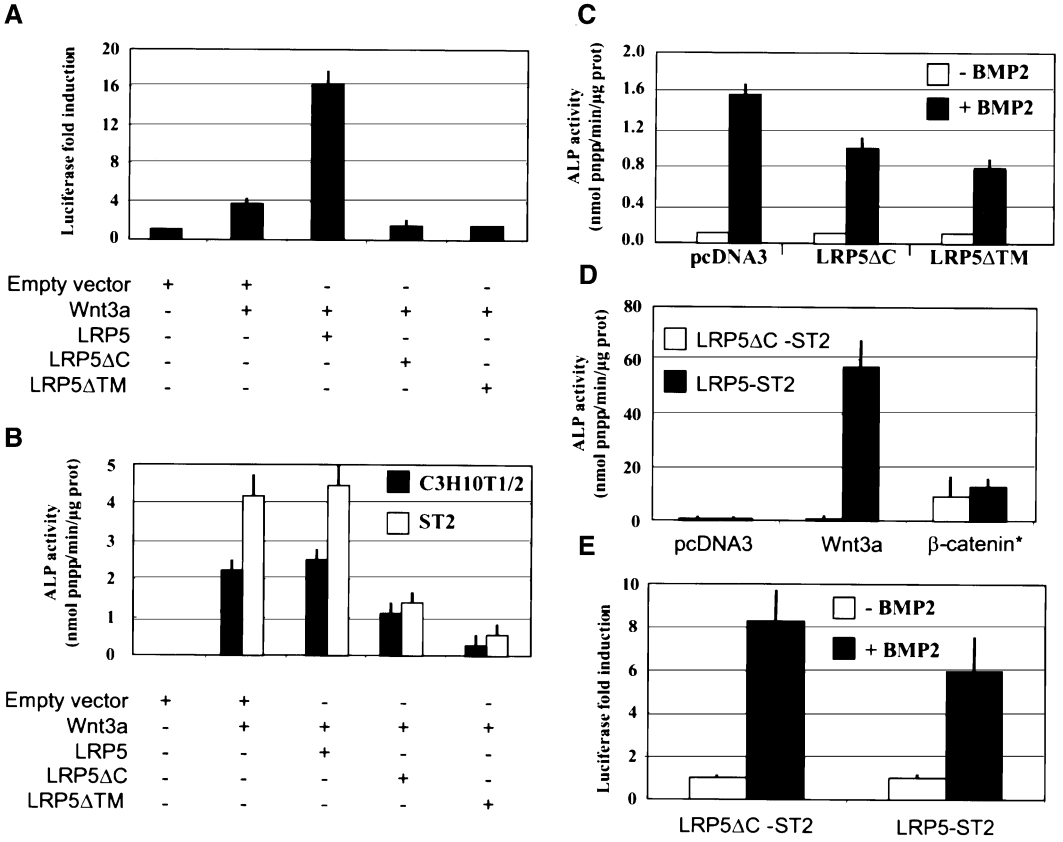

Figure 6. Dominant-Negative Forms of LRP5 Inhibit ALP Activity Induced by Wnt3a and BMP2

(A) COS-7 cells were transiently cotransfected with TCF-1, TOPflash, pTK-Renilla, and Wnt3a expression constructs. Where indicated, empty vector, LRP5, LRP5ΔC, or LRP5ΔTM expression constructs were added to the cotransfection mix. Luciferase activity was determined in cell lysates 24 hr after transfection and normalized to *Renilla* signal. Wild-type LRP5 increases Wnt3a-stimulated luciferase induction, whereas the mutant forms of LRP5 do not.

(B) C3H10T1/2 and ST2 cells were transiently cotransfected with Wnt3a and LRP5, LRP5ΔC, or LRP5ΔTM expression constructs. ALP activity was measured in cell lysates 72 hr after transfection and normalized to protein level. The dominant-negative forms of LRP5 reduce Wnt3a stimulation of ALP activity in these cells.

(C) ST2 cells were transiently transfected with empty vector (pcDNA3), LRP5ΔC, or LRP5ΔTM expression constructs. Sixteen hours after transfection, cells were left untreated (−BMP2) or treated with BMP2 at 100 ng/ml (+BMP2) and cultured for an additional 72 hr. ALP activity was measured in cell lysates and normalized to protein level. The dominant-negative forms of LRP5 reduce BMP2 stimulation of ALP activity in these cells.

(D) ST2 cell lines that are stably expressing LRP5ΔC (LRP5ΔC-ST2) or wild-type LRP5 (LRP5-ST2) were transiently transfected with Wnt3a expression vector or empty vector. ALP activity was determined in cell lysates 72 hr after transfection and normalized to protein level. There is less Wnt3a-induced ALP activity in cells stably expressing the dominant-negative form of LRP5.

(E) ST2 cell lines that are stably expressing LRP5ΔC (LRP5ΔC-ST2) or wild-type LRP5 (LRP5-ST2) were transiently cotransfected with Gal4-Smad1 expression construct, Gal4/luciferase reporter construct, and pTK-Renilla. Sixteen hours after transfection, cells were either left untreated (−BMP2) or treated with BMP2 at 100 ng/ml (+BMP2) for 24 hr. Luciferase activity was determined in cell lysates and normalized to *Renilla* level. There is no difference in Smad1-stimulated luciferase activity in cells stably expressing either wild-type or dominant-negative LRP5. All the aforementioned experiments were performed in triplicate and each was repeated three times. Data ± one SD from representative experiments is presented.

tant, both LRP5ΔC-ST2 and LRP5-ST2 cells were able to increase ALP activity, indicating that the β-catenin pathway is still functioning and that LRP5ΔC inhibitory activity is upstream in this pathway (Figure 6D). Finally, when we measured Smad1 transcriptional activity by using a GalSmad1-based one-hybrid assay, we found that LRP5ΔC-ST2 cells and LRP5-ST2 cells responded almost identically to the stimulation of BMP2 (Figure 6E). Therefore, the inability of LRP5ΔC-ST2 cells to respond to BMP2 is not due to an alteration in the BMP2 signaling pathway. Altogether our data suggest that the integrity of Wnt/LRP5 signaling is necessary for the induction of alkaline phosphatase in these cells.

Conditioned Media Containing the Dominant-Negative Secreted Form of LRP5 Reduces Bone Accrual in Calvarial Explant Cultures

While pluripotent mesenchymal cell lines can be induced into the osteoblastic lineage, they may not reflect endogenous osteoblastic proliferation and differentiation. Consequently, we sought to determine whether the secreted form of LRP5 (LRP5ΔTM) could interfere with bone accrual in calvarial explant cultures. In three independent experiments, explants that were cultured in the presence of conditioned media from cells expressing LRP5ΔTM consistently had thinner bone, as determined by ALP staining and von Kossa staining, than did ex-

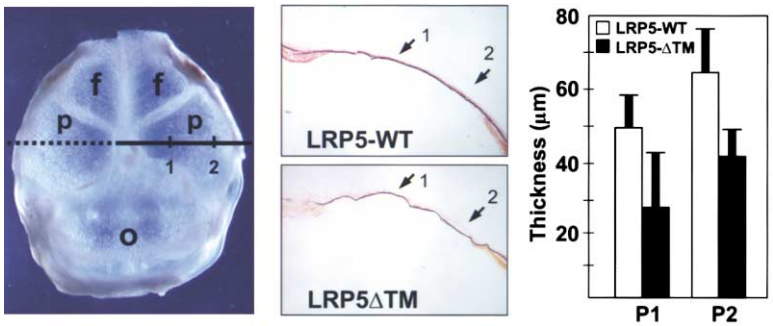

Figure 7. A Secreted Mutant Form of LRP5 Reduces Bone Formation in Calvarial Explants

(Left) Calvarial explants were cultured for 5 days in conditioned medium derived from LRP5-WT- or LRP5ΔTM-transfected COS-7 cells. A semidarkfield photograph depicts a typical calverium after 5 days in culture. The parietal (p), frontal (f), and occipital (o) bones are noted. Coronal sections of the explants were obtained midway through the parietal bones (level of section is depicted by black line).

(Middle) Representative coronal sections through the left parietal bone demonstrate less von Kossa staining (thickness of black areas by arrows) in explants cultured in LRP5ΔTM conditioned media versus LRP5-WT-conditioned media.

(Right) Mean thickness (± one SD) at two sites (P1 and P2) in five explants cultured in LRP5ΔTM-conditioned media is reduced in comparison to five explants cultured in LRP5-WT-conditioned media ($p < 0.01$).

plants that were cultured in conditioned media from cells expressing wild-type LRP5 (Figure 7). Thus, LRP5ΔTM is able to inhibit bone growth, presumably by binding and interfering with secreted growth factors such as Wnts.

Discussion

Bone Mass and Eye Development Are Affected by LRP5

We have shown that mutations in *LRP5* affect bone mass in humans. The recessive effect includes a severe reduction in bone mass and ocular pathology, the osteoporosis-pseudoglioma syndrome (Figure 1), while the dominant effect appears to be reduced bone mass in obligate carriers (Table 1). The mechanism of mutational effect of the OPPG disease-causing mutations is likely to be loss-of-function (Figure 2). Several independent observations suggest that LRP5 regulates osteoblastic proliferation or differentiation. First, the phenotype manifests during growth when osteoblastic anabolic activity supersedes osteoclastic catabolic activity. Second, *Lrp5* is expressed by developing and mature osteoblasts in situ (Figure 3). Third, *Lrp5* expression levels change as cells differentiate along the osteoblastic lineage in vitro (Figure 4). Dong et al. (1998) observed that LRP5 expression levels differed in three osteoblast-like tumor cell lines. The authors speculated that these differences might reflect each tumor cell line being arrested at a different stage of osteoblastic differentiation, although epigenetic changes altering gene expression in these cells could not be excluded. Our data supports modulation of LRP5 expression during osteoblastic differentiation. It is of interest that a Mendelian genetic high-bone-mass phenotype and a bone mass quantitative trait locus have also been mapped to genetic intervals that contain *LRP5* (Johnson et al., 1997; Koller et al., 1998). Since reduced LRP5 expression appears to negatively regulate bone mass, it is intriguing to speculate that other mutations or common polymorphisms, which affect the expression or activity of LRP5, will positively regulate bone mass.

LRP5 and Its Closely Related Superfamily Members Are Involved in Wnt Signal Transduction

LRP5 has two closely related paralogs, LRP6 in mammals and Arrow in *Drosophila*, which have been implicated in the Wnt signaling cascade (Pinson et al., 2000; Wehrli et al., 2000). Arrow transduces *Wg* signaling as a coreceptor with Frizzled and is upstream in the *Wg*-signaling cascade from the cytoplasmic second messengers Dishevelled, Lef, and β-catenin (Wehrli et al., 2000). Mice homozygous for an insertion mutation at the *Lrp6* locus have multiple developmental defects (Pinson et al., 2000) and resemble mice with targeted mutations of individual Wnt genes that signal via the canonical pathway (Uusitalo et al., 1999).

We used pluripotent mesenchymal cells that could be induced into the osteoblastic lineage by exogenous growth factors (Figure 4) to show that the Wnt/β-catenin signaling pathway can act upon these cells in a Smad-independent manner (Figure 5). We further showed that LRP5 is involved in this pathway, since reducing LRP5 function with either a transmembrane-anchored dominant-negative receptor or a secreted decoy receptor interfered with Wnt-induced ALP stimulation (Figure 6). Therefore, our data support other functional studies that put LRP5 in the Wnt signaling cascade (Mao et al., 2001; Tamai et al., 2000), and we extend these results by placing LRP5 and Wnt signaling in the cell differentiation pathway and tissue affected by LRP5 loss-of-function mutations.

We also observed a dosage effect for LRP5 function since heterozygous carriers of OPPG mutations can have reduced bone mass. Dosage effects are not unique to LRP5. Individuals who are heterozygous for LDL receptor loss-of-function mutations have the autosomal dominant phenotype familial hypercholesterolemia (Brown and Goldstein, 1986). Also, Pinson et al. (2000) observed a worsening of the vestigial tail phenotype (a hypomorphic Wnt3a allele) when it was moved onto a heterozygous *Lrp6* loss-of-function background.

The Wnt family member(s) involved in LRP5-mediated signaling during bone growth remain to be elucidated. By using TCF activation in COS cells and ALP activity in osteoblastic cells, we could demonstrate a functional interaction between LRP5 and Wnt family members that signal via the canonical pathway, such as Wnt3a and Wnt1, but not between LRP5 and Wnt family members that utilize other signaling pathways, such as Wnt5a. It is satisfying that *Alpl* is a downstream target of LRP5 signaling, since naturally occurring *ALPL* deficiency in humans and induced *Alpl* deficiency in mice also leads

to osteopenia and fractures (Fedde et al., 1999; Mornet, 2000; Wennberg et al., 2000). Several other genes with roles in bone biology have also been reported as targets of Wnt/β-catenin signaling (Ai et al., 2000; Globus et al., 1998; Gradl et al., 1999; Haertel-Wiesmann et al., 2000; Horiuchi et al., 1999; Jochum et al., 2000; Mann et al., 1999; Moursi et al., 1996). Therefore, deficiency of LRP5 may affect the expression of a series of genes that are important during bone formation.

LRP5 is also important during eye development. The OPPG phenotype in humans suggests that there is a defect in the involution of the primary vitreal vasculature that normally begins during the 13th gestational week (Ko et al., 1985; Zhu et al., 2000); failure of this process leads to fibrosis and contracture. We suspect that the transient expression of LRP5 by cells within the vitreal vasculature, or perhaps by other vitreous constituents, is responsible for this involution process. In the mouse, where regression of the primary vitreal vasculature occurs postnatally (Ito and Yoshioka, 1999), we were unable to detect LRP5 expression in E17.5 vitreal vessels. LRP5 may have very low levels of expression in these vessels, may have transient expression that is too brief to reliably observe, or may be expressed in low-abundance cells, such as vitreal macrophages. An essential role for vitreal macrophages in triggering vitreal vessel regression has been described (Lang and Bishop, 1993). Two other Mendelian genetic ocular disorders, autosomal dominant familial exudative vitreoretinopathy (FEVR) and autosomal dominant neovascular inflammatory retinopathy (VRNI), also map to an interval containing LRP5 (Li et al., 1992; Stone et al., 1992). Visual loss is a common feature in both syndromes, although there is variable expression and obligate carriers can be asymptomatic. Eye abnormalities have not been described in parents of patients affected with OPPG, although they have not been systematically sought. The pathogenesis of visual loss in OPPG appears distinct from that observed in FEVR and VRNI; however, LRP5 expression has also been detected in retinal tissue (Figueroa et al., 2000), and therefore it is reasonable to speculate that *LRP5* mutations could cause FEVR or VRNI via different mechanisms of mutational effect.

LRP5 Loss-of-Function Mutations Cause a Restricted Phenotype Despite Broad Expression

LRP5 is expressed in several tissues, as determined by Northern blot analysis (Dong et al., 1998; Hey et al., 1998; Kim et al., 1998), immunohistochemistry (Figueroa et al., 2000), and in situ hybridization (Figueroa et al., 2000). Therefore, it is surprising that the phenotypic consequences of mutation are restricted to the skeleton and the eye. As suggested by Pinson et al. (2000), it is possible that LRP6, which is also broadly expressed, has functional redundancy with LRP5 in many tissues. It is reasonable to consider that LRP5 may also bind and internalize multiple ligands in a non-signal-transducing capacity, similar to many other LDL receptor family members (Gliemann, 1998; Hussain et al., 1999). Evidence to support this conjecture is that LRP5 can bind ApoE-enriched low-density lipoproteins and that LRP5 expression increases in the livers of LDL receptor-deficient mice (Kim et al., 1998). Therefore, other LDL receptor family members may provide functional redundancy for LRP5 at other sites with respect to ligand binding and internalization. Since the sole postnatal consequence of LRP5 deficiency in humans is reduced bone accrual, it is exciting to speculate that the pharmacological modulation of LRP5 signaling in healthy individuals could positively affect peak bone mass and thereby reduce the risk for developing clinically significant osteoporosis in later life.

Experimental Procedures

Clinical Assessment, Genotyping, and Mutational Analysis

The study had the approval of the Institutional Review Board at University Hospitals of Cleveland. The diagnosis of OPPG was based upon the cooccurrence of congenital- or juvenile-onset eye disease and low bone mass. Other genetic and environmental causes of visual loss and low bone mass were excluded based on careful physical examination and laboratory testing. DNA from peripheral blood and total RNA from cultured patient skin fibroblasts or EBV-transformed lymphoblasts were extracted following standard methods. A percutaneous iliac crest bone biopsy was performed and analyzed with standard methods (Glorieux et al., 2000; Parfitt et al., 1987) and compared to age-matched controls (Glorieux et al., 2000). Polymorphic genetic markers were tested with established methods (Gong et al., 1996). Primer pairs were designed to PCR amplify LRP5 cDNA and all 23 coding exons from genomic DNA (primer sequences and conditions are available from the authors). PCR amplification was performed with standard methods and amplimers were sequenced directly. All identified mutations were confirmed at the genomic DNA level and were heterozygous in the patients' parents. In families with identified disease-causing mutations, an unaffected sibling's carrier status was determined by mutation detection. In other families, a sibling's carrier status was determined by linkage. Putative disease-causing missense mutations were not found in >50 control DNA alleles; however, control DNA was not matched for ancestry.

Quantitative Lumbar Spine Areal Bone Mineral Density Measurement

Areal bone mineral density (g/cm^2) of the lumbar spine (AP projection) was measured by dual-energy X-ray absorptiometry (DEXA). Participants were studied in different countries using different DEXA systems. Therefore, for statistical analyses each measure was converted to a standard deviation score (z score) relative to appropriate age- and gender-matched controls for the system that was used. Statistically significant differences between the study groups' mean z scores and control means ($z = 0$) were determined using Student's t test.

In Situ Hybridization

C57BL/6 wild-type mouse embryos were fixed in 4% paraformaldehyde in 0.1 M phosphate buffer (PB) (pH 7.4) at 4°C overnight. After immersion in 20% sucrose in PB, tissues were embedded in OCT compound, and frozen tissue sections were cut at a thickness of 8 μm. Limbs from a 1-month-old mouse were fixed in 4% paraformaldehyde for 5 days and decalcified in 0.5 M EDTA (pH 7.4) for 15 days. After dehydration, tissues were embedded in paraffin and sections were cut at a thickness of 5 μm. Tissues were deparaffinized and dehydrated before the in situ procedure.

Lrp5-specific antisense probes were synthesized to cover 700 base pairs of cDNA upstream of the unique EcoRI site. Digoxigenin-11-UTP-labeled single-strand ribo-probes were prepared with the DIG RNA-labeling kit (Roche) by in vitro transcription according to the manufacturer's protocol.

Hybridization was carried out as described (Bohme et al., 1995). Hybridization was detected using 4-nitroblue tetrazolium, 5-bromo-4-chloro-3-indyl-phosphate (X-phosphate), and nitroblue tetrazolium salt (NBT) as substrates for alkaline phosphatase at 4°C for 8 hr. After counter staining with 0.2% methyl-green, slides were allowed to

dry and mounted with Glycergel (DACO). The specimens were observed and recorded by a SPOT camera (Diagnostic Instruments).

BMP2 Induction of ST2 Cell Osteoblastic Differentiation

The murine bone marrow stromal cell line ST2 was cultured in RPMI 1640 (Cellgro) supplemented with 10% FBS, 50 U/ml penicillin, and 50 μg/ml streptomycin (GIBCO-BRL). Cells were plated at a density of $2 \times 10^4/cm^2$ in 25 cm^2 flasks, and when confluent, osteoblastic differentiation was induced by the addition of recombinant human BMP2 (Aventis) at 300 ng/ml. Cell cultures were then continued for up to 144 hr. Total RNA from cells was harvested at 0, 0.5, 1, 2, 3, 4, and 6 days following BMP2 addition by the use of the Trizol reagent (GIBCO-BRL), following the manufacturer's protocol.

Northern Blot Analysis

Total RNA isolated from cultured cells was separated in 1% agarose-formaldehyde gels (5 μg total RNA/ lane) and transferred to Hybond-N membrane (Amersham Pharmacia) via standard methods. We made replicate Northern blots to minimize potential differences in observed mRNA expression associated with repeat hybridization. Equal loading across gels and transfer to membrane was determined by ethidium bromide staining. Hybridization was performed overnight by Ultrahyb (Ambion), following the manufacturer's protocol. cDNA probes were random prime labeled by standard methods. Analyzed mouse probes included *Lrp5* nt 4101–5092 (GenBank accession #NM_008513), *Lrp6* nt 2918–3769 (GenBank accession #NM_008514), *Alpl*, *Bglap*, *Col1a1* (Sabatakos et al., 2000), and *Actb*.

LRP5 Expression Constructs and Stable LRP5-Expressing Cell Lines

LRP5 expression constructs were made with the pcDNA3 expression vector (Invitrogen). Full-length cDNA was amplified by RT-PCR from human fibroblasts and subcloned. A FLAG antibody epitope was inserted into the wild-type construct after nucleotide 165 (the insertion site is relative to the "A" in the ATG translation start site) using QUIKChange (Stratagene). QUIKChange was also used to create expression constructs containing the E1270fs and Q853X disease-causing mutations. Endogenous Pml I and Apa I restriction sites were used to generate the LRP5ΔC and LRP5ΔTM dominant-negative receptors, respectively. All constructs were confirmed by sequencing. Stable ST2 cell lines expressing either wild-type or an LRP5ΔC construct, generated by an endogenous BsrG I restriction enzyme site, were generated following G418 selection.

Generation of Wnt- and LRP5-Conditioned Media

The Wnt3a-expressing cell lines have been described (Shibamoto et al., 1998; Tamai et al., 2000). Cells were maintained in DMEM containing 10% FBS. Wnt3a (10 ml) containing culture media were collected every 2 days from 100 mm diameter culture dishes after the cells became confluent.

LRP5-conditioned media was generated by transiently transfecting 80% confluent COS-7 cells in 100 mm diameter dishes with 5 μg expression plasmid DNA using Fugene 6 (Roche) following the manufacturer's protocol. Conditioned medium (10 ml) was collected at 24 and 48 hr after the cells recovered from the transfection. The presence of the protein in conditioned media or cell extract was confirmed by Western blotting with the anti-FLAG antibody. From 10 ml of conditioned media and from 1 ml of cell lysate, 10 μl of each were separated by SDS-PAGE.

Wnt, Constitutive-Active β-Catenin, TCF-1, TCF-Luciferase, Gal4-Smad, and Gal4-Luciferase Constructs

Murine Wnt1, Wnt2, Wnt3a, Wnt4, Wnt5a, and Disheveled dominant-negative cDNAs were subcloned into the expression vector pcDNA3.1. Human β-catenin was RT-PCR amplified, confirmed by sequencing, and subcloned into pcDNA3.1. QUIKChange was used to create a constitutive active form of β-catenin (β-catenin*) with the S33Y missense mutation (Morin et al., 1997). Mouse TCF-1 was amplified by RT-PCR, cloned into pcDNA3.1, and confirmed by sequencing. The TCF-luciferase reporter construct TOPflash (van de Wetering et al., 1997) was obtained from Upstate Biotechnology. Smad1 one-hybrid vectors, Gal4-Smad1 expression construct, and Gal4/luciferase reporter were constructed as described (Spinella-Jaegle et al., 2001).

Wnt and LRP5 Responsiveness Using C3H10T1/2, ST2, and COS-7 Cell Lines

C3H10T1/2, ST2, and COS-7 cell lines were cultured (37°C, 5% CO_2), respectively, in α-MEM, RPMI, and DMEM medium supplemented with 10% heat-inactivated FBS. ST-2 stable cell lines were maintained in the corresponding culture medium and supplemented with G418 (500 μg/ml). For treatment or transient transfection, cells were plated at $2 \times 10^4/cm^2$, and 24 hr later treatment or transfections were carried out as indicated below.

Cells plated in 24 well plates were transiently transfected with the indicated construct (1 μg) using Fugene 6 (Roche). For luciferase reporter assays, 20 ng of pRL-TK (Promega), which encodes a *Renilla* luciferase gene downstream of a minimal HSV-TK promoter, was systematically added to the transfection mix to assess transfection efficiency. When required, controls utilized the corresponding empty vectors. Sixteen hours after transfection, cells were washed, cultured in media containing 2% FBS, and either left unstimulated or stimulated with BMP2 (100 ng/ml) for an additional 48 hr. Luciferase or ALP activity was determined in cell lysates.

When luciferase reporter constructs were used, luciferase assays were performed with the Dual Luciferase Assay Kit (Promega) according to the manufacturer's instructions. Cell lysate (10 μl) was assayed first for firefly luciferase and then for *Renilla* luciferase activity. Firefly luciferase activity was normalized to *Renilla* luciferase activity.

ALP activity was determined in cell lysates by the Alkaline Phosphatase Opt kit (Roche Molecular Biochemicals). Cell lysates were analyzed for protein content by using the micro-BCA Assay kit (Pierce), and ALP activity was normalized for total protein concentration.

Each experiment was performed in triplicate and was repeated three times.

Isolation and Culture of Mouse Calvarial Explants

Calvaria were obtained from 1-day-old Swiss Webster outbred mice (Taconic Farms). Skin and brain were dissected away. Whole calvaria were placed upside down in organ culture dishes (Falcon 3037) on a bed of 1.0% Seakem GTG agarose gel (FMC). A shallow depression conforming to the shape of the calvarial explant had been made before the agarose solidified by placing a glass bead on the agarose surface. The calvaria explants were then covered by a thin layer of 1% agarose. The agarose was dissolved in α-MEM (GIBCO-BRL) containing 10% FBS, 100 μg/ml ascorbic acid (Sigma), 5.0 mM β-glycero-phosphate (Sigma), 50 U/ml penicillin, and 50 μg/ml streptomycin. The explants were incubated with 2 ml of conditioned medium containing 100 μg/ml ascorbic acid and 5.0 mM β-glycerophosphate. Medium was changed on days 1 and 3. The samples were harvested at day 5, fixed with 4% PFA, and embedded in OCT compound. Serial coronal sections, including bilateral parietal bones, were cut at 7 μm thickness. ALP staining and von Kossa staining were performed, and pictures were taken with a SPOT camera. Thickness of the parietal bone at 1.2 mm (P1) and 2.4 mm (P2) from the midline was measured on ALP-stained sections.

Acknowledgments

We thank our patients and their families for participating in this research; Ms. B. Vayssière, Ms. C. Bartels, Ms. D. Schelling, and Ms. R. Travers for excellent technical assistance; and Drs. B. Grimes, H. Willard, M. Hebert, S. Chandrasekharappa, N. Katsanis, R, Nüsse, M. Semenov, D.L Shi, P. Byers, G. Wallis, and S. Takada for sharing reagents and scientific expertise. This work has been supported by the Osteogenesis Imperfecta Foundation, the March of Dimes Birth Defects Foundation, National Natural Science Foundation of China (39870409), Aventis Pharmaceuticals, and the Shriners of North America. M.L.W. is a recipient of a Clinician Scientist Award in Traditional Research from the Burroughs Wellcome Fund and is an Assistant Investigator with the Howard Hughes Medical Institute.

Received April 2, 2001; revised September 25, 2001.

References

Ai, Z., Fischer, A., Spray, D.C., Brown, A.M., and Fishman, G.I. (2000). Wnt-1 regulation of connexin43 in cardiac myocytes. J. Clin. Invest. *105*, 161–171.

Aubin, J.E. (1998). Advances in the osteoblast lineage. Biochem. Cell Biol. *76*, 899–910.

Bafico, A., Liu, G., Yaniv, A., Gazit, A., and Aaronson, S.A. (2001). Novel mechanism of Wnt signalling inhibition mediated by Dickkopf-1 interaction with LRP6/Arrow. Nat. Cell Biol. *3*, 683–686.

Bohme, K., Li, Y., Oh, P.S., and Olsen, B.R. (1995). Primary structure of the long and short splice variants of mouse collagen XII and their tissue-specific expression during embryonic development. Dev. Dyn. *204*, 432–445.

Brown, M.S., and Goldstein, J.L. (1986). A receptor-mediated pathway for cholesterol homeostasis. Science *232*, 34–47.

Chen, D., Lathrop, W., and Dong, Y. (1999). Molecular cloning of mouse Lrp7(Lr3) cDNA and chromosomal mapping of orthologous genes in mouse and human. Genomics *55*, 314–321.

Dong, Y., Lathrop, W., Weaver, D., Qiu, Q., Cini, J., Bertolini, D., and Chen, D. (1998). Molecular cloning and characterization of LR3, a novel LDL receptor family protein with mitogenic activity. Biochem. Biophys. Res. Commun. *251*, 784–790.

Fedde, K.N., Blair, L., Silverstein, J., Coburn, S.P., Ryan, L.M., Weinstein, R.S., Waymire, K., Narisawa, S., Millan, J.L., MacGregor, G.R., and Whyte, M.P. (1999). Alkaline phosphatase knock-out mice recapitulate the metabolic and skeletal defects of infantile hypophosphatasia. J. Bone Miner. Res. *14*, 2015–2026.

Figueroa, D.J., Hess, J.F., Ky, B., Brown, S.D., Sandig, V., Hermanowski-Vosatka, A., Twells, R.C., Todd, J.A., and Austin, C.P. (2000). Expression of the type I diabetes-associated gene LRP5 in macrophages, vitamin A system cells, and the Islets of Langerhans suggests multiple potential roles in diabetes. J. Histochem. Cytochem. *48*, 1357–1368.

Gliemann, J. (1998). Receptors of the low density lipoprotein (LDL) receptor family in man. Multiple functions of the large family members via interaction with complex ligands. Biol. Chem. *379*, 951–964.

Globus, R.K., Doty, S.B., Lull, J.C., Holmuhamedov, E., Humphries, M.J., and Damsky, C.H. (1998). Fibronectin is a survival factor for differentiated osteoblasts. J. Cell Sci. *111*, 1385–1393.

Glorieux, F.H., Travers, R., Taylor, A., Bowen, J.R., Rauch, F., Norman, M., and Parfitt, A.M. (2000). Normative data for iliac bone histomorphometry in growing children. Bone *26*, 103–109.

Gong, Y., Vikkula, M., Boon, L., Liu, J., Beighton, P., Ramesar, R., Peltonen, L., Somer, H., Hirose, T., Dallapiccola, B., et al. (1996). Osteoporosis-pseudoglioma syndrome, a disorder affecting skeletal strength and vision, is assigned to chromosome region 11q12–13. Am. J. Hum. Genet. *59*, 146–151.

Gradl, D., Kuhl, M., and Wedlich, D. (1999). The Wnt/Wg signal transducer beta-catenin controls fibronectin expression. Mol. Cell. Biol. *19*, 5576–5587.

Haertel-Wiesmann, M., Liang, Y., Fantl, W.J., and Williams, L.T. (2000). Regulation of cyclooxygenase-2 and periostin by Wnt-3 in mouse mammary epithelial cells. J. Biol. Chem. *275*, 32046–32051.

Hey, P.J., Twells, R.C., Phillips, M.S., Nakagawa, Y., Brown, S.D., Kawaguchi, Y., Cox, R., Xie, G., Dugan, V., Hammond, H., et al. (1998). Cloning of a novel member of the low-density lipoprotein receptor family. Gene *216*, 103–111.

Horiuchi, K., Amizuka, N., Takeshita, S., Takamatsu, H., Katsuura, M., Ozawa, H., Toyama, Y., Bonewald, L.F., and Kudo, A. (1999). Identification and characterization of a novel protein, periostin, with restricted expression to periosteum and periodontal ligament and increased expression by transforming growth factor beta. J. Bone Miner. Res. *14*, 1239–1249.

Huang, L.F., Fukai, N., Selby, P.B., Olsen, B.R., and Mundlos, S. (1997). Mouse clavicular development: analysis of wild-type and cleidocranial dysplasia mutant mice. Dev. Dyn. *210*, 33–40.

Hussain, M.M., Strickland, D.K., and Bakillah, A. (1999). The mammalian low-density lipoprotein receptor family. Annu. Rev. Nutr. *19*, 141–172.

Ito, M., and Yoshioka, M. (1999). Regression of the hyaloid vessels and pupillary membrane of the mouse. Anat. Embryol. *200*, 403–411.

Jochum, W., David, J.P., Elliott, C., Wutz, A., Plenk, H., Matsuo, K., and Wagner, E.F. (2000). Increased bone formation and osteosclerosis in mice overexpressing the transcription factor Fra-1. Nat. Med. *6*, 980–984.

Johnson, M.L., Gong, G., Kimberling, W., Recker, S.M., Kimmel, D.B., and Recker, R.B. (1997). Linkage of a gene causing high bone mass to human chromosome 11 (11q12–13). Am. J. Hum. Genet. *60*, 1326–1332.

Katagiri, T., Yamaguchi, A., Komaki, M., Abe, E., Takahashi, N., Ikeda, T., Rosen, V., Wozney, J.M., Fujisawa-Sehara, A., and Suda, T. (1994). Bone morphogenetic protein-2 converts the differentiation pathway of C2C12 myoblasts into the osteoblast lineage. J. Cell Biol. *127*, 1755–1766.

Kim, D.H., Inagaki, Y., Suzuki, T., Ioka, R.X., Yoshioka, S.Z., Magoori, K., Kang, M.J., Cho, Y., Nakano, A.Z., Liu, Q., et al. (1998). A new low density lipoprotein receptor related protein, LRP5, is expressed in hepatocytes and adrenal cortex, and recognizes apolipoprotein E. J. Biochem. *124*, 1072–1076.

Ko, M.K., Chi, J.G., and Chang, B.L. (1985). Hyaloid vascular pattern in the human fetus. J. Pediatr. Ophthalmol. Strabismus *22*, 188–193.

Koller, D.L., Rodriguez, L.A., Christian, J.C., Slemenda, C.W., Econs, M.J., Hui, S.L., Morin, P., Conneally, P.M., Joslyn, G., Curran, M.E., et al. (1998). Linkage of a QTL contributing to normal variation in bone mineral density to chromosome 11q12–13. J. Bone Miner. Res. *13*, 1903–1908.

Lang, R.A., and Bishop, J.M. (1993). Macrophages are required for cell death and tissue remodeling in the developing mouse eye. Cell *74*, 453–462.

Li, Y., Muller, B., Fuhrmann, C., van Nouhuys, C.E., Laqua, H., Humphries, P., Schwinger, E., and Gal, A. (1992). The autosomal dominant familial exudative vitreoretinopathy locus maps on 11q and is closely linked to D11S533. Am. J. Hum. Genet. *51*, 749–754.

Lu, P.W., Cowell, C.T., Lloyd-Jones, S.A., Briody, J.N., and Howman-Giles, R. (1996). Volumetric bone mineral density in normal subjects, aged 5–27 years. J. Clin. Endocrinol. Metab. *81*, 1586–90.

Mann, B., Gelos, M., Siedow, A., Hanski, M.L., Gratchev, A., Ilyas, M., Bodmer, W.F., Moyer, M.P., Riecken, E.O., Buhr, H.J., and Hanski, C. (1999). Target genes of beta-catenin-T cell-factor/lymphoid-enhancer-factor signaling in human colorectal carcinomas. Proc. Natl. Acad. Sci. USA *96*, 1603–1608.

Mao, J., Wang, J., Liu, B., Pan, W., Farr, G.H., 3rd, Flynn, C., Yuan, H., Takada, S., Kimelman, D., Li, L., and Wu, D. (2001). Low-density lipoprotein receptor-related protein-5 binds to Axin and regulates the canonical Wnt signaling pathway. Mol. Cell *7*, 801–809.

Morin, P.J., Sparks, A.B., Korinek, V., Barker, N., Clevers, H., Vogelstein, B., and Kinzler, K.W. (1997). Activation of beta-catenin-Tcf signaling in colon cancer by mutations in beta-catenin or APC. Science *275*, 1787–1790.

Mornet, E. (2000). Hypophosphatasia: the mutations in the tissue-nonspecific alkaline phosphatase gene. Hum. Mutat. *15*, 309–315.

Moursi, A.M., Damsky, C.H., Lull, J., Zimmerman, D., Doty, S.B., Aota, S., and Globus, R.K. (1996). Fibronectin regulates calvarial osteoblast differentiation. J. Cell Sci. *109*, 1369–1380.

NIH Consensus Development Panel on Osteoporosis Prevention, Diagnosis, and Therapy (2001). Osteoporosis prevention, diagnosis, and therapy. JAMA *285*, 785–795.

Parfitt, A.M., Drezner, M.K., Glorieux, F.H., Kanis, J.A., Malluche, H., Meunier, P.J., Ott, S.M., and Recker, R.R. (1987). Bone histomorphometry: standardization of nomenclature, symbols, and units. Report of the ASBMR histomorphometry nomenclature committee. J. Bone Miner. Res. *2*, 595–610.

Pinson, K.I., Brennan, J., Monkley, S., Avery, B.J., and Skarnes, W.C. (2000). An LDL-receptor-related protein mediates Wnt signalling in mice. Nature *407*, 535–538.

Riggs, B.L., and Melton, L.J. (1986). Involutional osteoporosis. N. Engl. J. Med. *314*, 1676–1686.

Roodman, G.D. (1996). Advances in bone biology: the osteoclast. Endocr. Rev. *17*, 308–332.

Sabatakos, G., Sims, N.A., Chen, J., Aoki, K., Kelz, M.B., Amling, M., Bouali, Y., Mukhopadhyay, K., Ford, K., Nestler, E.J., and Baron, R. (2000). Overexpression of DeltaFosB transcription factor(s) increases bone formation and inhibits adipogenesis. Nat. Med. *6*, 985–990.

Seeman, E., Tsalamandris, C., Formica, C., Hopper, J.L., and McKay, J. (1994). Reduced femoral neck bone density in the daughters of women with hip fractures: the role of low peak bone density in the pathogenesis of osteoporosis. J. Bone Miner. Res. *9*, 739–743.

Semenov, M.V., Tamai, K., Brott, B.K., Kuhl, M., Sokol, S., and He, X. (2001). Head inducer Dickkopf-1 is a ligand for Wnt coreceptor LRP6. Curr. Biol. *11*, 951–961.

Shibamoto, S., Higano, K., Takada, R., Ito, F., Takeichi, M., and Takada, S. (1998). Cytoskeletal reorganization by soluble Wnt-3a protein signalling. Genes Cells *3*, 659–670.

Shimizu, H., Julius, M.A., Giarre, M., Zheng, Z., Brown, A.M., and Kitajewski, J. (1997). Transformation by Wnt family proteins correlates with regulation of beta-catenin. Cell Growth Differ. *8*, 1349–1358.

Spinella-Jaegle, S., Rawadi, G., Kawai, S., Gallea, S., Faucheu, C., Mollat, P., Courtois, B., Bergaud, B., Ramez, V., Blanchet, A.M., et al. (2001). Sonic Hedgehog increases the commitment of pluripotent mesenchymal cells into the osteoblastic lineage and abolishes adipocytic differentiation. J. Cell Sci. *114*, 2085–94.

Stone, E.M., Kimura, A.E., Folk, J.C., Bennett, S.R., Nichols, B.E., Streb, L.M., and Sheffield, V.C. (1992). Genetic linkage of autosomal dominant neovascular inflammatory vitreoretinopathy to chromosome 11q13. Hum. Mol. Genet. *1*, 685–689.

Tamai, K., Semenov, M., Kato, Y., Spokony, R., Liu, C., Katsuyama, Y., Hess, F., Saint-Jeannet, J.P., and He, X. (2000). LDL-receptor-related proteins in Wnt signal transduction. Nature *407*, 530–535.

Uusitalo, M., Heikkila, M., and Vainio, S. (1999). Molecular genetic studies of Wnt signaling in the mouse. Exp. Cell Res. *253*, 336–348.

van de Wetering, M., Cavallo, R., Dooijes, D., van Beest, M., van Es, J., Loureiro, J., Ypma, A., Hursh, D., Jones, T., Bejsovec, A., et al. (1997). Armadillo coactivates transcription driven by the product of the Drosophila segment polarity gene dTCF. Cell *88*, 789–799.

Wehrli, M., Dougan, S.T., Caldwell, K., O'Keefe, L., Schwartz, S., Vaizel-Ohayon, D., Schejter, E., Tomlinson, A., and DiNardo, S. (2000). arrow encodes an LDL-receptor-related protein essential for Wingless signalling. Nature *407*, 527–530.

Wennberg, C., Hessle, L., Lundberg, P., Mauro, S., Narisawa, S., Lerner, U.H., and Millan, J.L. (2000). Functional characterization of osteoblasts and osteoclasts from alkaline phosphatase knockout mice. J. Bone Miner. Res. *15*, 1879–1888.

Yamaguchi, A., Ishizuya, T., Kintou, N., Wada, Y., Katagiri, T., Wozney, J.M., Rosen, V., and Yoshiki, S. (1996). Effects of BMP-2, BMP-4, and BMP-6 on osteoblastic differentiation of bone marrow-derived stromal cell lines, ST2 and MC3T3–G2/PA6. Biochem. Biophys. Res. Commun. *220*, 366–371.

Zhu, M., Madigan, M.C., van Driel, D., Maslim, J., Billson, F.A., Provis, J.M., and Penfold, P.L. (2000). The human hyaloid system: cell death and vascular regression. Exp. Eye Res. *70*, 767–776.